DOI: 10.1002/zaac.200600035

Chemical Bonding and Solid State NMR of Alkali Metal Monostannides MSn (M = Li, Na, K, Rb, Cs)

Frank Haarmann*, Daniel Grüner, Viktor Bezugly, Helge Rosner, and Yuri Grin

Dresden, Max-Planck-Institut für Chemische Physik fester Stoffe

Received February 6th, 2006.

Dedicated to Professor Herbert Jacobs on the Occasion of his 70th Birthday

Abstract. The mono-stannides of the alkali metals were investigated by ^{119}Sn NMR spectroscopy and full-potential local-orbital method calculations of the electronic structure and calculations of the electron localization function. The ^{119}Sn NMR signal shift of LiSn is due to Knight shift whereas the signal shift in the series from the Na to the Cs mono-stannides is most probably caused by chemical shielding. This is in agreement with electronic structure calculations resulting in a metal like band structure for LiSn and in semiconductor like band structures for the Na to Cs mono-stannides. A decreasing asymmetry parameter and an increasing shift of the NMR signal with increasing radius of the cations indicates a change of the electronic structure within the series of the semiconducting mono-stannides. The electron localization function also shows differences of the electronic environment of the Sn atoms due to a rearrangement of the lone pairs. Furthermore, the electronic structure calculations indicate an increase of the molecular character of the Sn_4^{4-} ion with increasing radius of the cations for the Na to Cs compounds.

Keywords: Tin; Stannides; NMR(^{119}Sn); ELF

Introduction

The mono-stannides of the alkali metals may be in principle interpreted as Zintl phases [1]. They can be divided into two groups based on electronic properties and crystal structures. Lithium mono-stannide shows metallic conductivity [2] in contrast to the expected semiconducting behaviour of closed-shell Zintl compounds. Its crystal structure is built by puckered 2D Sn nets (Fig. 1). Four weak covalent Sn−Sn bonds were discussed for each of the two crystallographically independent Sn atoms in LiSn [3] instead of three bonds as expected for Sn anions (isoelectronic to group 15 elements). The other alkali metals Na to Cs form semiconducting mono-stannides [4, 5, 6]. At high temperature above 483 °C a second modification, α-Na_4Sn_4, is known [8]. We focused on the modification stable at ambient temperature, β-Na_4Sn_4, to study the gradual changes within the series of the isostructural M_4Sn_4 compounds. The origin of the different electronic properties and crystal structures of LiSn and M_4Sn_4 compounds may be due to the small size of the Li atoms compared to the other alkali metals. As discussed in several quantum mechanical studies [3, 7], this prevents a separation of the Sn_4^{4-} tetrahedra and results in the formation of two-dimensional four connected Sn nets.

In the crystal structure, slightly distorted tetrahedral Zintl anions Sn_4^{4-} are built by symmetry-equivalent three-bonded Sn atoms (Fig. 1). To account for this bonding situation we refer to these compounds as M_4Sn_4. The existence of the Sn_4^{4-} tetrahedron in the melt was observed by neutron diffraction experiments and modelled with molecular dynamic calculations [9, 10]. Reorientation of the anions and diffusion of the cations in the α-modification of Na_4Sn_4 were observed by NMR studies [11, 12] and confirmed by *ab initio* molecular dynamic calculations [13]. The anions are coordinated by two crystallographically independent cations: four M1 are located above the faces and four M2 above the edges of the tetrahedron. Further they are additionally coordinated by four M1 and four M2 atoms, that each Sn_4^{4-} tetrahedron is coordinated by 16 cations (Fig. 1).

A weak decrease of the bond lengths within the tetrahedron with increasing size of the cations and no systematic change of the angles was observed in the single-crystal X-ray diffraction studies [5, 6] (Table 1). A Raman spectroscopic investigation on the M_4Sn_4 compounds shows no general tendency of the vibration frequencies like that observed in the M_4Ge_4 compounds of the alkali metals [14].

NMR spectroscopy is sensitive on the bonding situation of the atoms and reflects locally the environments of the nuclei under investigation. These may be anisotropic and result in an orientation dependence of the interactions, which can be observed in ordered solid compounds.

* Dr. F. Haarmann
MPI für Chem. Physik fester Stoffe
Nöthnitzer Str. 40
D-01187 Dresden
E-mail: haarmann@cpfs.mpg.de

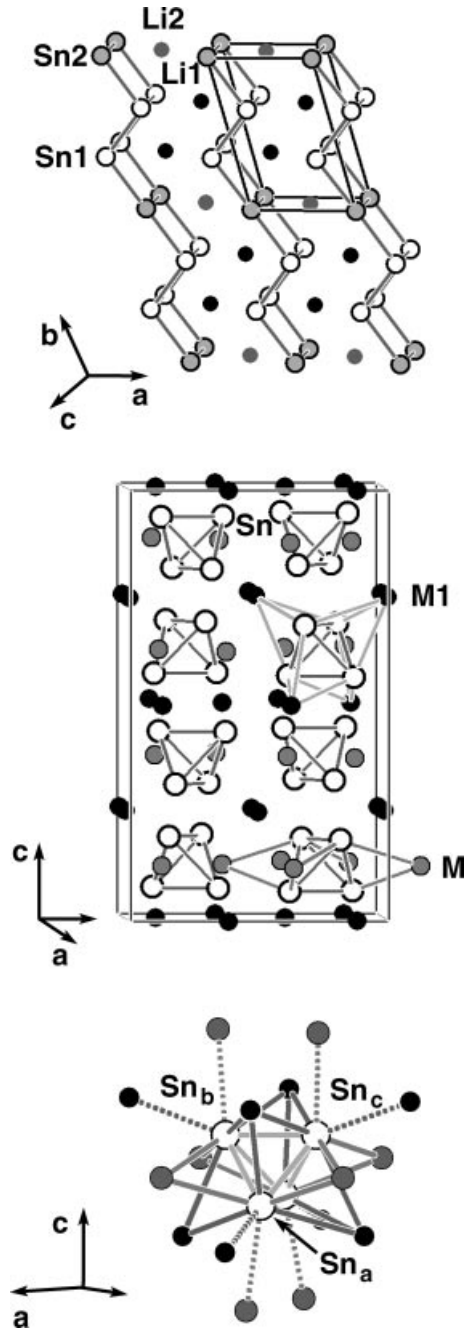

Fig. 1 Crystal structures of the alkali metal mono-stannides. (top) LiSn: The corrugated planes of Sn1 and Sn2 are highlighted by the grey bonds. (middle) M_4Sn_4 with M = Na, K, Rb, Cs: The intra molecular bonds of the Sn_4^{4-} tetrahedra are marked in grey. For clarity only one of the M1 and M2 coordination shells of the Sn atoms is exemplarily drawn. The unit cell marked with black lines is shifted by ($^1/_4$ 0 0) with respect to the standard setting of the space group $I4_1/acd$. (bottom) Atomic environment of the Sn_4^{4-} tetrahedron.

Whereas, fast molecular motion as in liquid- and gas phase or in dynamically disordered solids leads to a loss of this information [15, 16]. The exact calculation of chemical shielding in the solid state with heavy nuclei is still a problem [17, 18]. Only few studies focus on the calculation of NMR signal shifts in intermetallic compounds with metallic conductivity and these are devoted to light elements [19, 20].

In the present work, the structural pecularities of the alkali metals monostannides are investigated by combined application of solid state ^{119}Sn NMR spectroscopy and chemical bonding analysis by electronic band structure calculations and electron localization function.

Table 1 Lattice parameters, distances and bonding angles of the Sn_4^{4-} tetrahedra for the stannides M_4Sn_4 (space group $I4_1/acd$). The distances $d1$(Sn_b-Sn_c), $d2$(Sn_a-Sn_b) and the angles α(Sn_b-Sn_a-Sn_c), β(Sn_a-Sn_b-Sn_c) are defined according to Figure 1, bottom.

Compound	a/Å	c/Å	$d1$/Å	$d2$/Å	$d1/d2$	α/°	β/°
Na_4Sn_4	10.475(1)	17.514(2)	2.981(2)	2.975(2)	1.002	60.14	59.93
K_4Sn_4	11.409(1)	18.649(2)	2.954(1)	2.947(1)	1.002	60.17	59.91
Rb_4Sn_4	11.757(1)	19.215(2)	2.944(2)	2.942(2)	1.001	60.04	59.97
Cs_4Sn_4	12.122(1)	19.820(2)	2.944(2)	2.940(2)	1.001	60.09	59.95

Experimental Details

Preparation and Characterisation

The compounds were synthesized by melting of the appropriate mixtures of the pure elements (Li 99.4 % Alfa Aesar, Na 99.95 % Alfa Aesar, K 99.95 % Chempur, Rb 99.75 % Alfa Aesar, Cs 99.95 % Chempur, Sn 99.999 % Chempur) in tantalum ampoules and subsequent thermal annealing. Due to their sensitivity against moisture and oxygen all samples were handled in a glove box under argon. From X-ray powder diffraction all samples were determined as single phase. (STOE-STADIP-MP, $CuK_{\alpha 1}$ radiation, λ = 1.540598 Å) The literature values of unit cell parameters and atomic coordinates were used for calculation of interatomic distances and bond angles (Table 1).

NMR experiments

The NMR experiments were done at a Bruker AVANCE system (Rheinstetten, Germany) with a magnetic field of B_0 = 11.74 T, corresponding to a resonance frequency of about 186.502 MHz for ^{119}Sn. The signals are referenced to that of tetramethyl tin.

The frequency range accessible within a single FT NMR experiment is influenced by the quality factor (Q) of the HF circuit usually dominated by the probe and the duration of the pulses. A low Q wide line probe (NMR service, Erfurt, Germany) with a Manganin coil was used for the measurements. For wide line NMR measurements the samples were sealed in Pyrex glass tubes (5 mm diameter). Although all measurements were carried out at ambient temperature the probe was mounted on a JANIS cryostat system (Wilmington, USA). Magic angle spinning (MAS) measurements on LiSn were done with a Bruker standard double resonance probe with ZrO_2 rotors of 4 mm in diameter as sample container. To prevent eddy currents the powders of compounds with metallic conductivity were admixed with GeO_2 in a volume ratio of about 1/10. An eight-fold Hahn Echo sequence with short pulses of 1.5 µs and 3 µs duration was used for the detection of the signals. The short pulses were chosen to prevent signal distortion by long dur-

Table 2 Atomic sphere radii (in Å) used in TB-LMTO-ASA calculations.

	Na_4Sn_4	K_4Sn_4	Rb_4Sn_4	Cs_4Sn_4
M1	2.119	2.358	2.450	2.549
M2	2.076	2.297	2.387	2.483
Sn	1.713	1.765	1.783	1.796

ation of the pulses, accepting the loss of intensity due to the imperfect excitation of the nuclei. The inter-pulse interval was set to 60 μs to prevent a distortion of the signal in the measurements without rotation of the sample. In the MAS experiments, the pulses were synchronized with the rotation frequency. The parameters to describe the signals were determined by least squares methods using the SIMPSON program package [21]. Spin lattice relaxation times were measured using a saturation recovery sequence with detection by a Hahn Echo.

Calculation procedures

Electronic band structure calculations were carried out using the full-potential local-orbital minimum basis (FPLO) method [22] within the local-density approximation to density functional theory. In the scalar relativistic calculations the exchange and correlation potentials of *Perdew* and *Wang* [23] were used. As the basis set, Li(1*s*, 2*s*, 2*p*, 3*d*), Na(2*s*, 2*p*, 3*s*, 3*p*, 3*d*), K(3*s*, 3*p*, 3*d*, 4*s*, 4*p*, 4*d*), Rb(4*s*, 4*p*, 4*d*, 5*s*, 5*p*, 5*d*), Cs(5*s*, 5*p*, 5*d*, 6*s*, 6*p*, 6*d*), and Sn(4*s*, 4*p*, 4*d*, 5*s*, 5*p*, 5*d*) states were employed. The lower lying states were treated fully relativistic as core states. The Li 3*d*, Na 3*d*, K 4*d*, Rb 5*d*, Cs 6*d*, and Sn 5*d* states were taken into account as polarization states to increase the completeness of the basis set. The treatment of Li(1*s*), Na(2*s*, 2*p*), K(3*s*, 3*p*), Rb(4*s*, 4*p*), Cs(5*s*, 5*p*) semi-core like states as valence states was necessary to account for non-negligible core-core overlaps. A mesh of 512 k points in the irreducible part of the Brillouin zone was used to ensure accurate density of states and band structure information, especially in the region close to the Fermi level. We used the crystallographic parameters presented in refs. [5, 6] in our calculations.

Additionally, the TB LMTO ASA program package [24] with exchange correlation potential (LDA) according to von *Barth* and *Hedin* [25] was used. The radial scalar-relativistic Dirac equation was solved to get the partial waves. The calculation within the atomic sphere approximation (ASA) includes corrections for the neglect of interstitial regions and partial waves of higher order [26]. The atomic sphere radii were determined according to a standard procedure described in [27]. For comparison, we carried out additional calculations without empty spheres. Application of empty spheres did not improve decisively the total energy, thus ELF was calculated on the basis of self-consistent calculations without empty spheres. The atomic sphere radii used in the latter calculations are listed in Table 2. Basis sets containing the Sn(5*s*, 5*p*), Na(3*s*), K(4*s*), Rb(5*s*), and Cs(6*s*) orbitals were employed for the self-consistent calculations with the Sn(5*d*, 4*f*), Na(3*p*, 3*d*), K(4*p*, 4*d*), Rb(4*p*, 4*d*), and Cs(5*p*, 5*d*) functions being downfolded. The electron localization function (ELF) was evaluated according to [28] within the TB LMTO ASA program package with an ELF module already implemented, and was analyzed with the program Basin [29].

To clarify the influence of the close surrounding on the orientation of the lone pairs of the Sn atoms in the structure, the calculations of the electronic structure of an isolated Sn_4^{4-} tetrahedral molecule (d(Sn-Sn) = 2.978 Å) were done at the DFT level using the ADF program package [30]. The scalar relativistic approach [31], and Becke's gradient-corrected exchange-energy functional [32] and Lee, Yang, Parr's [33] gradient-corrected correlation-energy functional (BLYP) were employed here. The triple zeta basis set with two polarization functions (TZ2P) from the internal ADF basis set library was used. The subsequent ELF calculation was performed with the program DGrid [34].

Results and Discussion

LiSn

The ^{119}Sn NMR signals of the LiSn are shown in Figure 2. The large signal shift of about 5400 ppm is in the range of Knight shifts (K) and by far too large to result from chemical shielding (δ) being in the range of about -2000 ppm $\leq \delta \leq$ 600 ppm [35, 36]. The signal shift of LiSn is similar to that of the lithium transition metal stannides $LiAg_2Sn$, LiAuSn, Li_2AuSn, and $LiTSn_4$ with T = Ru, Rh, Ir varying from 3970 ppm $\leq K \leq$ 5300 ppm [37, 38, 39, 40] and is significantly smaller than for β-Sn with K = 7350 ppm [41]. The Knight shift is characteristic for metallic and semiconducting compounds and is due to the interaction of the nuclear spins and the spin of the mobile charge carriers. Only one ^{119}Sn NMR signal was observed by the wide line measurements instead of two as it could be expected from the number of non-equivalent Sn positions in the crystal structure. No further signals were detected in a frequency range of about ±1 MHz centred at the observed value. MAS experiments improved the resolution and resulted in a minor influence of the spinning on the line shape (Fig. 2 bottom). The width of the signal is reduced compared with the wide line spectrum but there is still overlap of the side bands and the centre band. This indicates local disorder in the crystal structure resulting either from vacancies or from an exchange of the Li and Sn atoms. The microscopic origin of the disorder in LiSn is not understood yet. However, the existence of the disorder is already indicated by the observation of a homogeneity range for $Li_{50+x}Sn_{50-x}$ with $0 \leq x \leq 1$ at T = 469 °C [2]. The isotropic shift of the signal could be determined in a series of experiments (Table 3). The large Q factor of the MAS probe restricts the accessible frequency range leading to a systematic distortion of the line shape.

The shape of the wide line signal resembles a spectrum due to the anisotropy of the Knight shift (Fig. 2). The agreement of a least squares fit applying one signal to the measurement is good. However, the site coordination of the two Sn positions differs which should result in two different NMR signals. Considering only the homonuclear coordination, the Sn2 atoms have square planar environment with d(Sn2-Sn2) = 3.18 Å (2×) and d(Sn2-Sn1) = 3.16 Å (2×), whereas the Sn1 atoms being also four-bonded posses non-planar environment desired from a tetrahedron with d(Sn1-Sn1) = 3.18 Å (2×) and d(Sn1-Sn2) = 3.16 Å (2×). Adding the lithium atoms into the coordination reduces the differ-

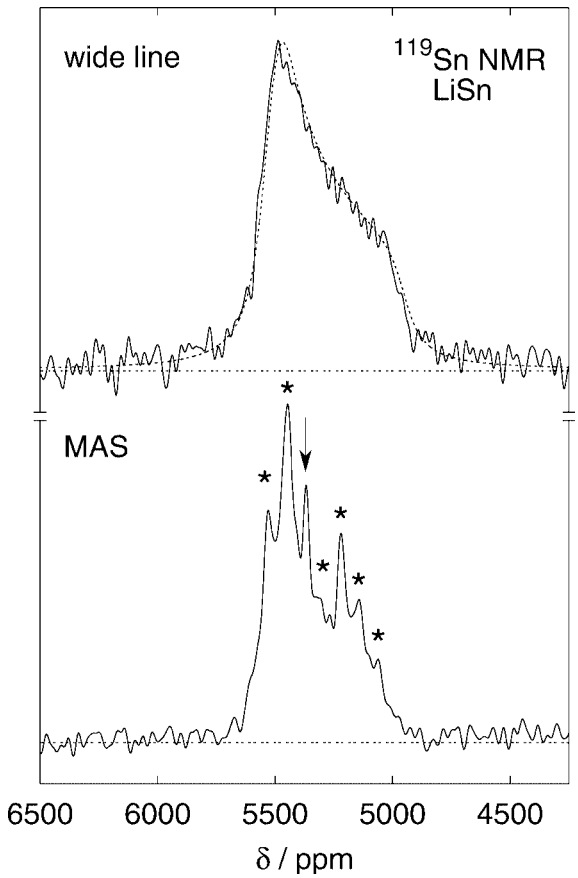

Fig. 2 ^{119}Sn NMR of LiSn. (top): Static wide line (full line) and simulated spectrum (dashed line). (bottom): MAS signal accumulated using a rotation frequency of 15 kHz. The isotropic frequency is marked by an arrow and the positions of the side bands by asterisks.

Table 3 NMR Parameter of the ^{119}Sn wide line signals of the alkali metal stannides determined by least square fitting of the profiles.

Compound	δ_{iso}/ppm	Δ/ppm	η	T_1/s
LiSn[a)]	~5400	–	–	–
Na_4Sn_4	−1371(5)	471(5)	0.43(2)	85(1)
K_4Sn_4	−1343(5)	566(5)	0.35(2)	96(1)
Rb_4Sn_4	−1189(5)	579(5)	0.32(2)	31(2)
Cs_4Sn_4	−784(5)	481(5)	0.26(2)	77(1)

[a)] Isotropic shift determined in a series of MAS experiments.

ences in the environment of the tin positions. Both become twelve-coordinated with cuboctahedron as coordination polyhedron for Sn2 and the hexagonal analogon of cuboctahedron for Sn1. The average distance to the next neighbours does not differ significantly ($\bar{d}$(Sn1-Sn) = 3.17 Å, $\bar{d}$(Sn2-Sn) = 3.17 Å, $\bar{d}$(Sn1-Li) = 3.04 Å, $\bar{d}$(Sn2-Li) = 3.05 Å). Observing only one signal may be due to various reasons: The signals corresponding to Sn1 and Sn2 are broadened by disorder and overlap, or a so far unobserved signal is too broad to be separated from the background.

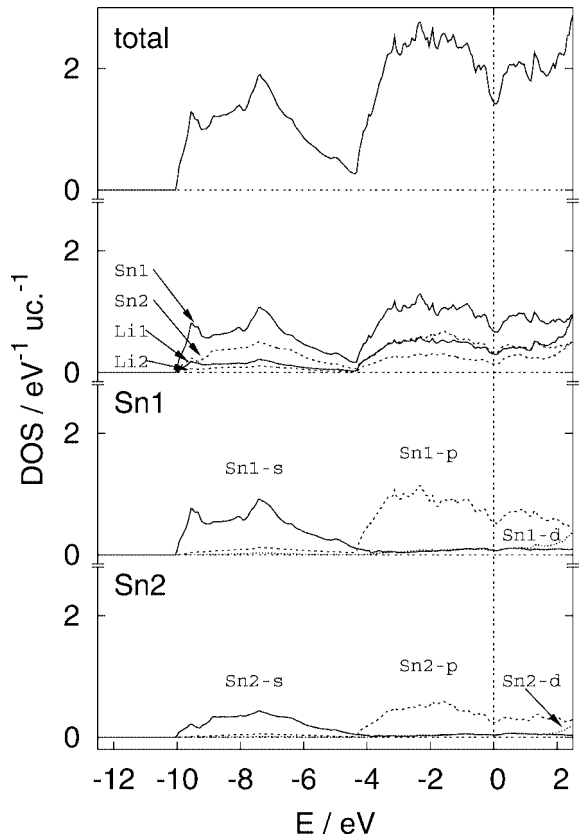

Fig. 3 Total electronic density of states (DOS) of LiSn. Full lines represent position Sn1/Li1 and dashed lines Sn2/Li2 contributions.

Both circumstances result in an unpredictable effect on the line shape and influence the fit parameter. This prevents the further determination of spectral parameters. The third reason for the signal overlap can be peculiarities of the electronic structure.

The electronic density of states of LiSn is depicted in Figure 3. Occupied states at the Fermi level clearly indicate the metallic character being in agreement with former investigations of conductivity [2] and the electronic structure [3, 7, 42]. The contributions of the individual atoms are also shown. While the DOS of the Li atoms are almost equal for both Li sites small differences can be seen for the Sn sites. The projected density of states shows a dominant *s*-like contribution of Sn atoms in the range from −10 eV to −4.5 eV. Above −4.5 eV the *p*-like contribution of the Sn atoms becomes dominant. Only a small fraction of the Sn *d*-states contributes to the DOS.

The *s*-projected density of states at the Fermi level for both Sn1 and Sn2 positions is about 0.04 eV^{-1} atom^{-1}. Assuming the Knight shift dominates the interaction of the ^{119}Sn nuclear moments with the magnetic field, the offset of the NMR signals should be similar for both sites according to the *s*-projected DOS values at Fermi level. This is in agreement with the observation of only one signal.

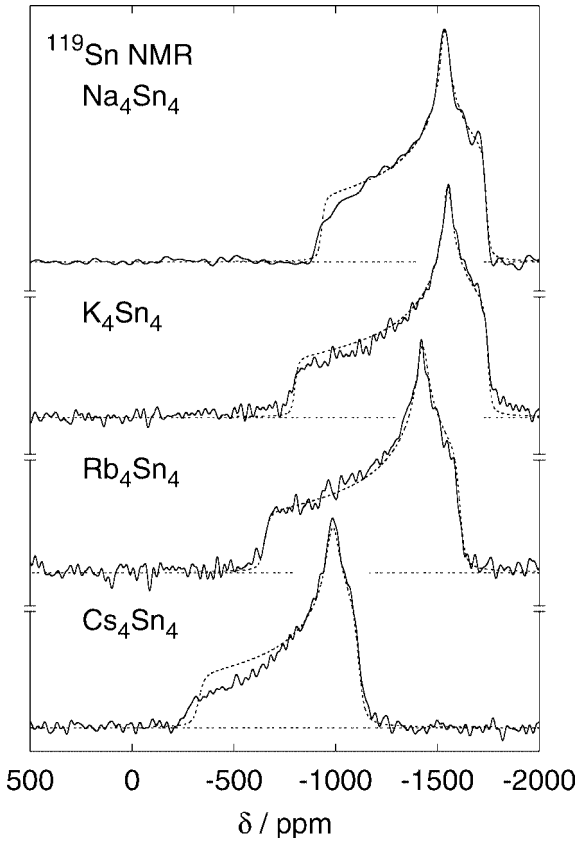

Fig. 4 ^{119}Sn NMR wide line signals of M_4Sn_4 with M = Na, K, Rb, Cs (full lines) and simulated spectra (dashed lines). The signal frequencies are referenced to tetramethyl tin.

M_4Sn_4 with M = Na, K, Rb, Cs

NMR experiments

The ^{119}Sn NMR signals of the alkali metal mono-stannides M_4Sn_4 (Fig. 4) are shifted towards low field with increasing atomic number and size of the cation indicating chemical shielding or core polarization as origin of the signal offset. It can principally not be distinguished from the line shape whether chemical shielding or core polarisation or a anisotropy of Knight shift is the dominant interaction. For this reason, the shape of the signals can be described by anisotropy of the chemical shielding tensor [15, 16]. The spectral parameters determined by least squares fitting of the profiles are summarized in Table 3. The anisotropy parameter (Δ) of the signals shows no general tendency whereas the asymmetry parameter (η) and the isotropic shift (δ_{iso}) of the signals decrease with increasing size of the cations.

The assumption of the dominant effect of chemical shielding seems to be justified by the missing temperature dependence of the ^{119}Sn signal shift of β-Na_4Sn_4 [11, 12]. If the interaction of the mobile charge carriers would be dominant a shift of the signal to higher frequencies with increasing temperature should be observed for a semiconducting compound [43]. If the chemical shielding is the dominant mechanism for the interaction of the nuclear moments with the magnetic field the charge of the anions and the hybridisation of the orbitals determine the line shape and the shift of the signals.

Following this interpretation the asymmetry parameter is a local probe for the symmetry of the charge distribution of the Sn atoms. The non-zero values of the asymmetry parameter in the experiment (Table 3) are in agreement with the deviation from the threefold symmetry at the Sn sites. The decrease of η for M_4Sn_4 with M = Na, K, Rb, Cs with increasing size of the cations should reflect a decrease of the deviation of the environment symmetry from the tetrahedral one.

Both crystallograpically independent Sn-Sn distances (*d1*, *d2*, Table 1) in the Sn_4^{4-} tetrahedra decrease with the size of the cation. Nevertheless, the ratio *d1*/*d2* as well as the bond angles α and β which should reflect the deformation of the tetrahedron do not change significantly with the cation and do not correlate with the changes of the NMR signal.

Therefore, to investigate the origin of the systematic variation of the NMR signals we analyzed the electronic band structure and the chemical bonding with electron localization function.

Electronic structure

The electronic density of states (DOS) for the M_4Sn_4 compounds is depicted in Fig. 5. The angular-momentum-decomposed DOS is exemplarily shown for β-Na_4Sn_4. Three groups of bands are located below the Fermi level for each of the compounds. The two at lowest energies are mainly formed by *s*-like contributions of the Sn atoms. The group below Fermi level is basically due to *p*-like Sn states and of a mixture of the alkali metals states. The lowest energy block of bands of Cs_4Sn_4 is due to a 5*p* contribution of the alkali metal. Corresponding contributions are at lower energies for the other compounds (M = Na, K, Rb). The gap between bonding and anti bondingstates is of about 0.4 eV for β-Na_4Sn_4 and 0.7 eV for the other monostannides of the alkali metals. Our results are in good agreement with calculations made with *ab initio* local density methods for Na_4Sn_4 and K_4Sn_4 [7].

The tendency of a narrowing of the Sn *s*, *p*-bands below the Fermi level with increasing size of the cations observed for Na_4Sn_4 and K_4Sn_4 [7] becomes more evident for Rb_4Sn_4 and Cs_4Sn_4 (Fig. 5). This can be interpreted by a more molecule-like electronic structure of the Sn_4^{4-} tetrahedron with increasing mass of the cation.

According to population analysis, the charge transfer is very small in the alkali metal mono-stannides. Furthermore, the direction of charge transfer differs within the series being from Sn to Na or K and in the opposite direction in the Rb and Cs compounds. This is in contradiction with the expectation of positively charged electropositive metals according the Zintl-Klemm-Busmann concept.

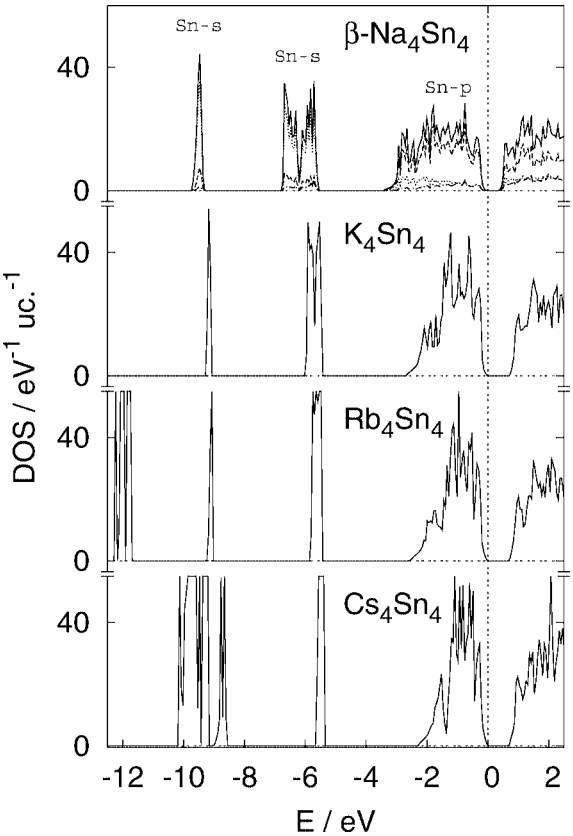

Fig. 5 Electronic density of states (DOS) of M_4Sn_4 with M = Na, K, Rb, Cs. Dotted lines represent the *s*-, dashed lines the *p*-, and dash-dotted lines the d-contributions to the angular-momentum-decomposed density of states.

Thus the non-quantitative analysis of the electronic band structure does not allow the interpretation of the systematic changes in the NMR for the M_4Sn_4 compounds. For further investigation of these tendencies we employed the bonding analysis in real space.

Electron density and electron localization function

For characterization of the chemical bonding in the M_4Sn_4 with M = Na, K, Rb, Cs compounds, we calculated the electron density and electron localization function serving as a bonding indicator in real space. Topological analysis of ELF and the electron density was performed in order to (a) evaluate the charge transfer from alkali metal cations to Sn_4 anions and (b) analyze chemical bonding in the vicinity of the Sn atoms.

The charge transfer from the alkali metal to the Sn atoms influences the shielding of the Sn nuclei. According to the Zintl-Klemm-Busmann concept the charge transfer should be complete in the M_4Sn_4 compounds, nevertheless a systematic variation of the ^{119}Sn NMR signal shift was observed. The decrease of the shielding with increasing radius of the cations may therefore indicate a partial charge transfer in the series of compounds. To clarify the trend within the M_4Sn_4 compounds, charge transfer was analyzed using *Bader*'s Atoms-In-Molecules approach [44] as well as an integration of electron density within the ELF basins (Table 4).

Table 4 Electron counts in M_4Sn_4 compounds (q in electrons per atom).

	q(Bader)			q(ELF)				
M	M1	M2	Sn	M1	M2	Sn(core)	Sn(valence)	Sn(total)
Na	10.3	10.3	50.9	10.1	10.1	45.9	5.2	51.1
K	18.3	18.3	50.8	18.1	18.1	45.9	5.2	51.1
Rb	36.3	36.3	50.8	36.2	36.2	45.9	5.1	51.0
Cs	54.4	54.4	50.8	54.2	54.3	45.9	5.0	50.9

From both methods for each of the compounds, the electron count for alkali metal positions on M1 and M2 sites are equal within numerical accuracy. With both methods, a transfer of nearly four electrons from the alkali metal atoms to the Sn_4^{4-} tetrahedron is observed for all M_4Sn_4 compounds. Thus, the change of the charge transfer cannot be the origin of the systematic variation of the NMR signal shift.

Bader analysis of the electron densities of M_4Sn_4 compounds results in a single maximum for each Sn atom being also center of gravity of the charge distribution of the corresponding basin. To study the chemical bonding in detail and its possible influence on their NMR behavior we apply the electron localization function. Despite the relatively complex crystal structures the topology of ELF in M_4Sn_4 reveals only three groups of attractors. The first group of attractors is in the core region of the atoms, which are close to spherical, and indicate, that the electrons of the outer core shells do not contribute to the bonding in the valence region [45]. Integration of the electron density in the basins of these attractors confirmed this suggestion. The electron counts for the outer core shells are in good agreement with the values obtained for isolated atoms [46]. The separation of the outer core shells of the alkali metals is very sharp (ELF < 0.1) which is characteristic for systems with strong charge transfer between the cationic and the anionic parts of the structure (cf. [47] for MgRhB). In the valence region, ELF shows disynaptic attractors located in vicinity of the Sn-Sn contacts (Fig. 6) indicating two-centre bonds. The electron count for these attractors increases slightly from sodium to caesium compound but remains clearly lower than two as expected from the Zintl count (Table 5). This can be understood from a comparison with elemental tin. The Sn-Sn distances in the M_4Sn_4 compounds (Table 1) are considerably larger than the interatomic distances d(Sn-Sn) = 2.81 Å in α-Sn. An ELF calculation for α-Sn reveals disynaptic attractors (Fig. 6) with a count of 2.1 electrons.

Beside the disynaptic bonding ELF attractors in the valence region of the M_4Sn_4 compounds a group of attractors appears, which are monosynaptic with respect to the tin atoms. They can be interpreted as 'lone-pair' like. For the isolated tetrahedral molecule Sn_4^{4-} there is only one such attractor located on the outer side of each tin atom on the

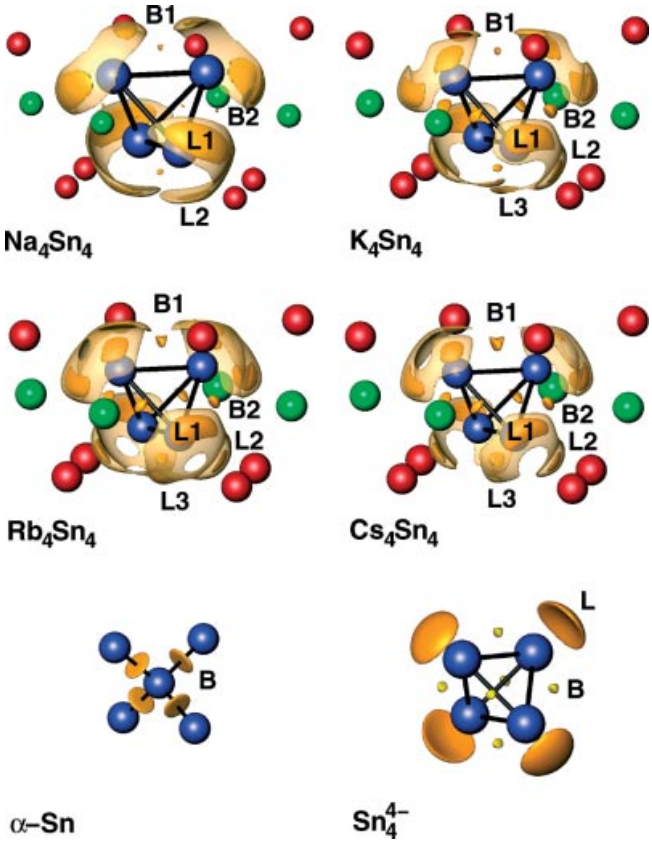

Fig. 6 Electron localization function for crystal structures of M_4Sn_4 (M = Na, K, Rb, Cs) in comparison with the isolated Sn_4^{4-} molecule and α-Sn (M1 red, M2 green, Sn violet). ELF isosurfaces are shown for the 'lone-pair' like attractors (L1, L2, L3) and the disynaptic attractors (B1, B2). ELF values of 0.65 (L1, L2), 0.593 (B1), 0.595 (B2) for Na_4Sn_4, 0.71, 0.71 (L1, L2), 0.652, 0.665, 0.693 (L3), 0.63, 0.65, 0.66 (B1, B2) for K_4Sn_4, Rb_4Sn_4, Cs_4Sn_4 were used. ELF values of 0.625, 0.65, 0.65, 0.66 highlight the transparent envelope of the 'lone-pair' attractors of Na_4Sn_4, K_4Sn_4, Rb_4Sn_4, Cs_4Sn_4. ELF isosurfaces for α-Sn with 0.6 (B), for Sn_4^{4-} with 0.7 (L) and 0.545 (B) are shown.

three fold axis (Fig. 6). Because of the non-tetrahedral cationic environment of the Sn_4^{4-} tetrahedron in the M_4Sn_4 compounds the 'lone-pair' attractor splits in two (Na_4Sn_4) or three (M = K, Rb, Cs). The attractor values (Table 6) are very close reflecting their common origin. The total electron count for these attractors changes systematically with M but remains much more than two expected from the Zintl count. The average distance from the attractor to the tin atoms (Table 6) increases slightly with the decreasing electron count (Table 5).

To compare the positions of the 'lone-pair' attractors in the M_4Sn_4 compounds we introduce a polar coordinate system where the *z* axis is along a line passing the position of a Sn atom and the centre of gravity of the tetrahedron (Fig. 7, top). The *x* axis is within the mirror plane of the molecule. The positions of the ELF maxima are compiled in Table 6 and are depicted in the polar diagram (Fig. 7, bottom). Na_4Sn_4 clearly differs from the other M_4Sn_4 compounds. The triangle resulting for M_4Sn_4 with M = K, Rb, Cs becomes more regular with increasing radius of the cations. This indicates a gradual decrease of the anisotropy of the charge distribution of the Sn atoms, corresponding to the observed decrease of the asymmetry parameter of the ^{119}Sn NMR signal in the series of compounds M_4Sn_4 from M = Na to M = Cs.

Table 5 Electron counts for ELF attractors in the valence region of M_4Sn_4 compounds.

M	Sn ('lone-pair')				Sn–Sn (bonds)	
	L1 (4×)	L2 (4×)	L3 (4×)	total	B1 (2×)	B2 (4×)
Na	2.6	1.7		4.3	0.6	0.6
K	1.6	1.2	0.9	3.7	0.8	1.1
Rb	1.5	1.1	0.9	3.5	0.9	1.1
Cs	1.4	0.9	0.9	3.2	1.0	1.3

Table 6 ELF attractors in M_4Sn_4 compounds.

Compound	Attractors and their values		Position θ/°	φ/°	Distance to Sn atoms d/Å	$\bar{d}$/Å
Na_4Sn_4	L1	0.679	56.5	344.9	1.65	1.61
	L2	0.658	66.2	155.6	1.57	
	B1	0.596	117.3	180.0	1.68	1.67
	B2	0.596	119.0	58.5	1.69	
	B2	0.596	118.0	298.3	1.63	
K_4Sn_4	L1	0.730	51.6	347.5	1.72	1.64
	L2	0.703	48.0	98.9	1.57	
	L3	0.659	73.5	193.8	1.62	
	B1	0.637	115.1	180.0	1.70	1.69
	B2	0.649	116.1	58.7	1.68	
	B2	0.649	116.0	298.5	1.68	
Rb_4Sn_4	L1	0.751	51.7	12.0	1.78	1.66
	L2	0.727	48.3	254.0	1.63	
	L3	0.679	59.5	147.5	1.58	
	B1	0.663	113.8	180.0	1.72	1.70
	B2	0.668	114.9	61.0	1.70	
	B2	0.668	114.9	301.0	1.70	
Cs_4Sn_4	L1	0.747	51.8	16.8	1.79	1.68
	L2	0.732	48.0	257.2	1.66	
	L3	0.659	50.5	130.6	1.60	
	B1	0.680	113.2	180.0	1.73	1.71
	B2	0.680	114.7	62.2	1.73	
	B2	0.681	113.7	302.2	1.68	

The differences in electron count for basins assigned to 'lone-pairs' or Sn–Sn bonds as well as the variation of ELF topology in the series M_4Sn_4 with M = Na, K, Rb, Cs lead to changes of the charge distribution of the Sn atoms (Table 6). These should influence the ^{119}Sn NMR signal shift and the anisotropy of the shielding. From our topological analysis of ELF it is evident that the most significant change in the bonding situation occurs in going from M = Na to M = K, whereas the M = K, Rb, Cs compounds exhibit a step by step modification of the charge distribution. The development of the asymmetry parameter shows the same tendency, whereas the isotropic shift changes most clearly in going from M = Rb to M = Cs.

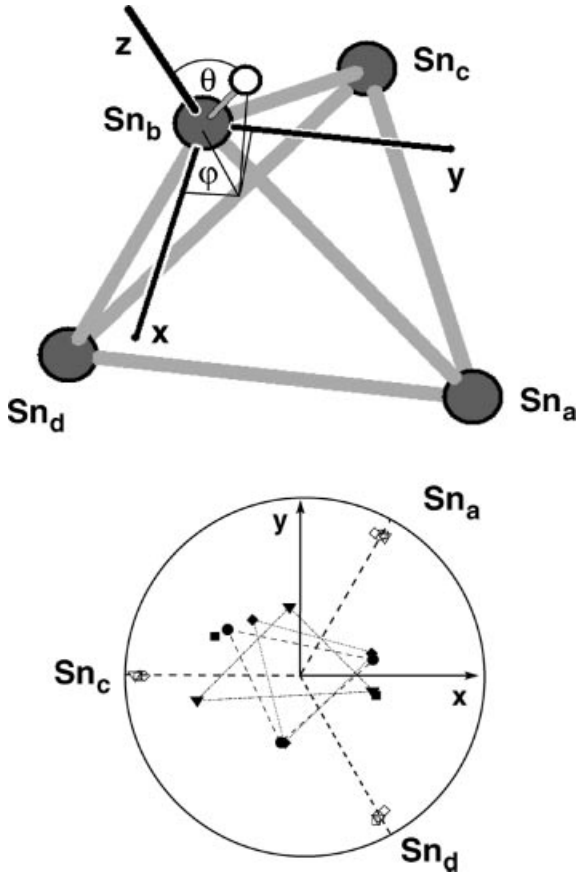

Fig. 7 (top): Coordinate system for the position of the 'lone-pair' attractors in M_4Sn_4 compounds (θ = polar angle, φ = azimuth) with respect to the Sn_4^{4-} tetrahedron. The position of an ELF maximum is indicated with a circle. (bottom) Position of the 'lone-pair' attractors in projection along *z* axis: Na_4Sn_4 as squares, K_4Sn_4 as triangles, Rb_4Sn_4 as circles, Cs_4Sn_4 as diamonds.

Conclusion

The different electronic band structure for metallic LiSn and semiconducting M_4Sn_4 with M = Na, K, Rb, Cs results in a difference of the ^{119}Sn NMR signal shift for both types of compounds. The large positive offset of the LiSn signal is due to the interaction of mobile charge carriers with the nuclear moments of the Sn atoms while the large negative shift of the signal of the M_4Sn_4 compounds with M = Na, K, Rb, Cs is most probably due to chemical shielding caused by the peculiarities of bonding interaction between the cations and anions and within the anions.

^{119}Sn NMR spectroscopy and an investigation of the ELF indicate a systematic change of the charge distribution of the Sn atoms for M_4Sn_4 with M = Na, K, Rb, Cs with increasing radius of the cations. From the NMR spectroscopy a systematic variation of the isotropic shift (δ_{iso}) and the asymmetry parameter (η) was observed. The tendency of η correlates with an analysis of ELF topology revealing systematic increase of regularity in the orientation of the maxima assigned to 'lone-pairs' and the redistribution of electron counts between 'lone-pairs' and bonding regions around the Sn atoms. The latter are in perfect agreement with the change of the interatomic distances within the Sn_4^{4-} tetrahedra.

Acknowledgement. We are thankful to *Dr. Michael Baitinger* and *Susann Leipe* for the assistance by the synthesis of the samples and *Dr. Raul Cardoso-Gil* for X-ray powder diffraction of the air-sensitive compounds. Furthermore, we acknowledge financial support of Emmy-Noether-Programm of the DFG (HR).

References

[1] F. Laves, *Naturwissenschaften* **1941**, *17*, 244.
[2] G. Grube, E. Meyer, *Z. Elekrochem.* **1934**, *40*, 771.
[3] A. Ienco, R. Hoffmann, G. Papoian, *J. Am. Chem. Soc.* **2001**, *123*, 2317.
[4] F. Springelkamp, R. A. de Groot, W. Geertsma, W. van der Lugt, F. M. Mueller, *Phys. Rev. B* **1985**, *32*, 2319.
[5] Yu. Grin, M. Baitinger, R. Kniep, H. G. von Schnering, *Z. Kristallogr. NCS* **1999**, *214*, 453.
[6] M. Baitinger, Yu. Grin, R. Kniep, H. G. von Schnering, *Z. Kristallogr. NCS* **1999**, *214*, 457.
[7] O. Genser, J. Hafner, *J. Phys.: Condens. Matter* **2001**, *13*, 959.
[8] W. Hume-Rothery, *J. Chem. Soc.* **1928**, *121*, 947.
[9] O. Genser, J. Hafner, *J. Phys.: Condens. Matter* **2001**, *13*, 981.
[10] M. Stolz, O. Leichtweiß, R. Winter, M. L. Saboungi, W. S. Howels, *Europhysics Lett.* **1994**, *27*, 221.
[11] R. D. Stoddard, M. S. Conradi, A. F. McDowell, M.-L. Saboungi, D. L. Price, *Phys. Rev. B* **1995**, *52*, 13998.
[12] R. D. Stoddard, M. S. Conradi, A. F. McDowell, M.-L. Saboungi, D. L. Price, *J. Non-Cryst. Sol.* **1996**, *205–207*, 203.
[13] L. M. Molina, M. J. López, J. A. Alonso, M. J. Stott, *Phys. Rev. B* **2003**, *68*, 174204.
[14] M. Somer, private communication.
[15] A. Abragam, Principles of Nuclear Magnetism, Oxford University Press, Oxford, New York 1961.
[16] C. P. Slichter, Principles of Magnetic Resonance, Springer-Verlag, Berlin, Heidelberg, New York, 3rd Ed., 1990.
[17] J. R. Yates, C. J. Pickard, M. C. Payne, *J. Chem. Phys.* **2003**, *118*, 5746.
[18] D. Sebastiani, *Mod. Phys. Lett. B* **2003**, *17*, 1301.
[19] V. P. Antropov, I. I. Mazin, O. K. Andersen, A. I. Lichtenstein, O. Jepsen, *Phys. Rev. B* **1993**, *47*, 12373.
[20] E. Pavarini, I. I. Mazin, *Phys. Rev. B* **2001**, *64*, 140504.
[21] M. Bak, J. T. Rasmussen, N. Ch. Nielsen, *J. Magn. Reson.* **2000**, *147*, 296.
[22] K. Koepernik, H. Eschrig, *Phys. Rev. B* **1999**, *59*, 1743.
[23] J. P. Perdew, Y. Wang, *Phys. Rev. B* **1992**, *45*, 13244.
[24] O. Jepsen, O. K. Andersen, The Stuttgart TB-LMTO-ASA program, Version 4.7, Max-Planck-Institut für Festkörperforschung, Stuttgart, 1999.
[25] U. von Barth, L. Hedin, *J. Phys. C* **1972**, *5*, 1629.
[26] O. K. Andersen, *Phys. Rev. B* **1975**, *12*, 3060.
[27] O. Jepsen, O. K. Andersen, *Z. Phys. B* **1995**, *97*, 35.
[28] A. Savin, H. J. Flad, J. Flad, H. Preuss, H. G. von Schnering, *Angew. Chem.* **1992**, *104*, 185; *Angew. Chem., Int. Ed. Engl.* **1992**, *31*, 185.
[29] M. Kohout, Basin, Version 3.1, Max-Planck-Institut für Chemische Physik fester Stoffe, Dresden, Germany, 2006.
[30] ADF2005.01, SCM, Theoretical Chemistry, Vrije Universiteit, Amsterdam, The Netherlands, http://www.scm.com.
[31] E. van Lenthe, E. J. Baerends, J. G. Snijders, *J. Chem. Phys.* **1993**, *99*, 4597.

[32] A. D. Becke, *Phys. Rev. A* **1988**, *38*, 3098.
[33] C. Lee, W. Yang, R. G. Parr, *Phys. Rev. B* **1988**, *37*, 785.
[34] M. Kohout, program DGrid, version 3.1, Max-Planck Institute for Chemical Physics of Solids, Dresden, 2005.
[35] J. Mason, Multinuclear NMR, Kluwer Academic/Plenum Publishers, 1987.
[36] D. Holland, A. P. Howes, R. Dupree, J. A. Johnson, C. E. Johnson, *J. Phys. Cond. Matt.* **2003**, *15*, 2457.
[37] Z. Wu, R.-D. Hoffmann, D. Johrendt, B. D. Mosel, H. Eckert, R. Pöttgen, *J. Mater. Chem.* **2003**, *13*, 2561.
[38] Z. Wu, H. Eckert, B. D. Mosel, M. H. Möller, R. Pöttgen, *Z. Naturforsch.* **2003**, *58b*, 501.
[39] Z. Wu, H. Eckert, J. Senker, D. Johrendt, G. Kotzyba, B. D. Mosel, H. Trill, R.-D. Hoffmann, R. Pöttgen, *J. Phys. Chem. B* **2003**, *107*, 1943.
[40] Z. Wu, B. D. Mosel, H. Eckert, R.-D. Hoffmann, R. Pöttgen, *Chem. Eur. J.* **2004**, *10*, 1558.
[41] J. Winter, Magnetic Resonance in Metals, Oxford University Press, 1971.
[42] O. Genser, J. Hafner, *Phys. Rev. B* **2001**, *63*, 144204.
[43] H. Selbach, O. Kanert, D. Wolf, *Phys. Rev. B* **1979**, *19*, 4435.
[44] R. F. W. Bader, Atoms in Molecules − A Quantum Theory, Clarendon Press, Oxford, 1995.
[45] M. Kohout, F. R. Wagner, Yu. Grin, *Theor. Chem. Acc.* **2002**, *108*, 150.
[46] M. Kohout, Die Elektronen-Lokalisierungs-Funktion und ionische Bindung, PhD Thesis, Universität Stuttgart 1999.
[47] A. M. Alekseeva, A. M. Abakumov, A. Leithe-Jasper, W. Schnelle, Yu. Prots, J. Hadermann, G. Van Tendeloo, E. V. Antipov, Yu. Grin, *Z. Anorg. Allg. Chem.* **2005**, *631*, 1047.

